

HIGH-LUNDQUIST NUMBER SCALING IN THREE-DIMENSIONAL SIMULATIONS OF PARKER'S MODEL OF CORONAL HEATING

C. S. NG

Geophysical Institute, University of Alaska Fairbanks, PO Box 757320, Fairbanks, AK 99775, USA

L. LIN AND A. BHATTACHARJEE

Space Science Center, University of New Hampshire, 39 College Road, Durham, NH 03824, USA

Accepted for publication in Astrophysical Journal

ABSTRACT

Parker's model is one of the most discussed mechanisms for coronal heating and has generated much debate. We have recently obtained new scaling results in a two-dimensional (2D) version of this problem suggesting that the heating rate becomes independent of resistivity in a statistical steady state [Ng and Bhattacharjee, *Astrophys. J.*, **675**, 899 (2008)]. Our numerical work has now been extended to 3D by means of large-scale numerical simulations. Random photospheric footpoint motion is applied for a time much longer than the correlation time of the motion to obtain converged average coronal heating rates. Simulations are done for different values of the Lundquist number to determine scaling. In the high-Lundquist number limit, the coronal heating rate obtained so far is consistent with a trend that is independent of the Lundquist number, as predicted by previous analysis as well as 2D simulations. In the same limit the average magnetic energy built up by the random footpoint motion tends to have a much weaker dependence on the Lundquist number than that in the 2D simulations, due to the formation of strong current layers and subsequent disruption when the equilibrium becomes unstable. We will present scaling analysis showing that when the dissipation time is comparable or larger than the correlation time of the random footpoint motion, the heating rate tends to become independent of Lundquist number, and that the magnetic energy production is also reduced significantly.

Subject headings: magnetic reconnection — magnetohydrodynamics (MHD) — Sun: corona — Sun: magnetic topology

1. INTRODUCTION

The enormous energy content of high-beta photospheric plasma flows has long been suggested as the source of energy that ultimately heats the million degree solar corona. Unambiguously identifying the exact mechanisms that transfer this kinetic energy into the overlying solar atmosphere and the exact nature of how the coronal magnetic field responds and converts this energy into heat remains one of the long-standing issues in astrophysics.

In this paper we investigate an idealized model of the corona proposed by Parker (1972) which applies to closed magnetic field structures whose field lines are embedded at both ends in the solar surface. Neglecting the curvature of the magnetic field, the corona is modeled in Cartesian geometry where an initially uniform magnetic field along the \hat{e}_z direction is line-tied at $z = 0$ and $z = L$ in perfectly conducting end-plates representing the photosphere. Parker suggests that slow and continuous random shuffling of the footpoints at these end-plates, representing the turbulent buffeting of the coronal field embedded in the convecting photosphere, can tangle the field into a braided structure of sufficient complexity such that it cannot settle into a continuous smooth equilibrium, but rather necessarily evolves to one with tangential discontinuities. Whether or not true current singularities (as opposed to current layers with finite

thickness) can form in this scenario and whether or not continuous footpoint mappings necessarily imply a non-smooth topology has been the subject of intense debate in the decades that have passed since Parker's seminal proposal. Extended discussion of this matter is beyond the scope of the present analysis, but it is appropriate to reiterate here (c.f. Ng & Bhattacharjee 1998) that this question is not merely of academic interest. That the plasma gradients will tend towards singularities has important bearing on the physics of magnetic reconnection and turbulence dynamics in the corona. The interested reader is referred to Ng & Bhattacharjee (1998), Low (2010), Huang et al. (2010), Janse, Low, & Parker (2010) and references therein.

In a process Parker calls "topological dissipation", it is at these tangential discontinuities where the corona's small but ultimately finite resistivity induce the formation of current sheets where magnetic energy is dissipated to heat the coronal plasma, and where magnetic reconnection proceeds to reduce the topological complexity of the coronal magnetic field. This essential concept was further developed in a series of studies (Parker 1979, 1983a,b, 1988, 1994) and has become known colloquially as the "nanoflare model" of coronal heating. The appellation derives from the isolation of 10^{23} erg flares as the constitutive energy release events which occur in "storms" of sufficient ferocity to heat the corona and adequately account for observed conductive and radiative losses. While the concept of topological dissipa-

tion can be seen as the prototypical “DC” mechanism for coronal heating (c.f. Klimchuk 2006; Aschwanden 2004), the solar atmosphere surely admits more complex magnetic topology than is treated by the Parker model. In fact, many investigators have pursued reconnection-based heating mechanisms using geometries that include separators, separatrixes and magnetic-nulls (see Priest et al. 2005, and references therein), and more recently by analyzing the magnetic topology of active regions observed by *Transition Region and Coronal Explorer* (Lee et al. 2010). It remains clear however, that coronal loops are the basic building block of the solar corona, and that their examination first as isolated entities is crucial in laying the foundations for a broader understanding of the corona and its activity (see Reale 2010 for a recent review).

The work we present here is motivated by a recent study (Ng & Bhattacharjee 2008, hereafter NB08) which developed a simplified version of the Parker scenario. NB08 referred to this version as a constrained tectonics model (Priest et al. 2002) because the random braiding at the line-tied ends was restricted to depend on only one coordinate transverse to the initial magnetic field. This strong assumption has the consequence that it enables us to describe the complete dynamics of the system by a simple set of differential equations which are easily amenable to analytical and numerical solutions for prescribed footpoint motion. The geometric constraints imposed by our assumption preclude the occurrence of nonlinear effects such as reconnection and secondary instabilities, but enables us to follow for long times the dissipation of energy due to the effects of resistivity and viscosity. Using this model, it was shown both numerically and by scaling analysis that as long as the correlation time of turbulent photospheric flow (τ_c) is much smaller than the characteristic resistive timescales (τ_R), ohmic dissipation becomes independent of resistivity (η). The absence of nonlinear effects in this model allows the perpendicular magnetic field (B_\perp) to grow to unphysically large values and is found to scale as $\eta^{-1/2}$. Furthermore, NB08 conjectured, by means of a heuristic scaling argument, that even in the presence of reconnection and secondary instabilities, the heating rate would remain insensitive to resistivity. It is this conjecture that we examine here using three-dimensional (3D) reduced MHD (RMHD) simulations.

The Parker model has been studied extensively using 3D MHD numerical simulations (Mikic et al. 1989; Longcope & Sudan 1994; Einaudi et al. 1996; Hendrix et al. 1996; Galsgaard & Nordlund 1996; Dmitruk et al. 1998; Gomez et al. 2000; Rappazzo et al. 2008, 2010 among others.) Here we are interested in the precise scaling of dissipation with respect to plasma resistivity. Our study is most similar in design to that of Longcope & Sudan (1994) who used RMHD to simulate Parker’s model with Lundquist numbers spanning an order or magnitude. In this range they found that both heating rate and perpendicular field production scales as $\eta^{-1/3}$. These numerical results agreed with analysis based on Sweet–Parker reconnection theory and measurements of current sheet statistics.

In this paper, we recover the scalings of heating rate and of B_\perp of Longcope & Sudan (1994) in the range

they examined, and extend their results to a range of lower η , where the results support a slower growth of B_\perp which roughly scales as $\eta^{-1/5}$ and a heating rate that becomes insensitive to η . We also demonstrate by simple scaling analysis that the transition between these scaling behaviors results from the diminishing effects of random photospheric motion as the energy dissipation timescale τ_E becomes much smaller than the correlation time τ_c , in accordance with NB08.

The paper is organized as follows. In Section 2 we describe the RMHD coronal heating model and numerical scheme. Section 3 gives the details of the simulation results. Section 4 presents a scaling analysis describing the transition in the observed scaling behavior. Section 5 summarizes our conclusions to date and discusses outstanding physical issues.

2. CORONAL HEATING MODEL AND NUMERICAL SETUP

We assume that the coronal plasma is sufficiently low-beta so that the dynamics can be described by the RMHD equations. Many numerical studies of Parker’s model mentioned above (with the notable exceptions of Galsgaard & Nordlund 1996; Gudiksen & Nordlund 2005; Peter et al. 2006) are based on the RMHD approximation. The RMHD equations are a simplified version of MHD applicable to systems where the plasma is dominated by a strong guide field such that the timescales of interest are slow compared with the characteristic Alfvén timescale τ_A . These restrictions also imply incompressibility ($\nabla \cdot \mathbf{v} = 0$) and the exclusion of magnetosonic modes (leaving only the shear Alfvén modes propagating in \hat{e}_z). The RMHD equations were first derived for the study of tokamak plasmas by Kadomtsev & Pogutse (1974) and Strauss (1976), which can be written in dimensionless form as

$$\frac{\partial \Omega}{\partial t} + [\phi, \Omega] = \frac{\partial J}{\partial z} + [A, J] + \nu \nabla_\perp^2 \Omega \quad (1)$$

$$\frac{\partial A}{\partial t} + [\phi, A] = \frac{\partial \phi}{\partial z} + \eta \nabla_\perp^2 A \quad (2)$$

where A is the flux function so that the magnetic field is expressed as $\mathbf{B} = \hat{\mathbf{e}}_z + \mathbf{B}_\perp = \hat{\mathbf{e}}_z + \nabla_\perp A \times \hat{\mathbf{e}}_z$; ϕ is the stream function so that the fluid velocity field is expressed as $\mathbf{v} = \nabla_\perp \phi \times \hat{\mathbf{e}}_z$; $\Omega = -\nabla_\perp^2 \phi$ is the z -component of the vorticity; $J = -\nabla_\perp^2 A$ is the z -component of the current density; and the bracketed terms are Poisson brackets such that, for example, $[\phi, A] \equiv \phi_y A_x - \phi_x A_y$ with subscripts here denoting partial derivatives. The normalized viscosity ν is the inverse of the Reynolds number R_ν , and resistivity η is the inverse of the Lundquist number S . The normalization adopted in Equations (1) and (2) is such that the magnetic field is in the unit of B_z (assumed to be a constant in RMHD); velocity is in the unit of $v_A = B_z/(4\pi\rho)^{1/2}$ with a constant density ρ ; length is in the unit of the transverse length scale L_\perp ; time t is in the unit of L_\perp/v_A ; η is in the unit of $4\pi v_A L_\perp/c^2$; and ν is in the unit of $\rho v_A L_\perp$.

In this paper we investigate an idealized model of the corona proposed by Parker (1972). In Parker’s model, a solar coronal loop is treated as a straight ideal plasma column, bounded by two perfectly conducting end-plates representing the photosphere. The footpoints of the magnetic field in the photosphere are frozen (line-tied). Ini-

tially, there is a uniform magnetic field along the z direction. The footpoints on the plates $z = 0$ and $z = L$ are subjected to slow, random motion $\phi(z = 0, t)$ and $\phi(z = L, t)$ that deform the magnetic field. The method we follow for imposing random footpoint motion is described in detail in Longcope (1993). We use a correlation time of $\tau_c = 10$. Only a band of Fourier modes with small k is driven so that the boundary flow is of the characteristic length scale of the order of the perpendicular simulation box size. The amplitude of the driving is small enough such that the root-mean-square boundary flow ($v_{\text{rms}} \sim 0.075$) is small compared with the Alfvén speed along the large-scale magnetic field.

The footpoint motion is assumed to take place on a timescale much longer than the characteristic time for Alfvén wave propagation between $z = 0$ and $z = L$, so that the plasma can be assumed to be in quasi-static equilibrium nearly everywhere, if such equilibrium exists, during this random evolution. For a given equilibrium, a footpoint mapping can be defined by following field lines from one plate to the other. Since the plasma is assumed to obey the ideal MHD equations, the magnetic field lines are frozen in the plasma and cannot be broken during the twisting process. Therefore, the footpoint mapping must be continuous for smooth footpoint motion. Parker (Parker 1972) claimed that if a sequence of random footpoint motion renders the mapping sufficiently complicated, there will be no smooth equilibrium for the plasma to relax to, and tangential discontinuities (or current sheets) of the magnetic field must develop. Although Parker’s claim has stimulated considerable debate, (see Janse, Low, & Parker 2010), we have shown elsewhere that it is valid if the equilibrium becomes unstable because there is only one smooth equilibrium for a given footpoint mapping (Ng & Bhattacharjee 1998) under RMHD and using periodic boundary conditions in transverse coordinates. Moreover, thin current layers generally do appear in numerical simulations with small but finite resistivity, after random boundary flows have been applied for a period of time.

Ordinarily, the problem of calculating time-dependent solutions of Equations (1) and (2) in line-tied magnetic field geometry involves all three spatial coordinates and time. As a first step in NB08, we had made a strong assumption that in addition to the coordinate z along which the magnetic field is line-tied, the dynamics depends on only one transverse coordinate x (as well as time t). The nonlinear terms (those that involve Poisson brackets) in RMHD equations (1) and (2) then become identically zero.

We have developed computer simulation codes that integrate Equations (1) and (2) numerically for arbitrary footpoint displacements in both 2D and 3D. We use spectral decomposition in x and y (using a standard two-thirds de-aliased pseudo-spectral method) and a leapfrog finite difference method in z on a staggered grid. The accuracy of the Fast Fourier Transform (FFT) routine used has been tested extensively as shown in Ng et al. (2008). For the 2D version, we can use an implicit method for time-integration so that we can take larger time steps than is allowed by the Courant-Friedrich-Lewy (CFL) condition for numerical stability of explicit methods, unlike in the 3D version, in which a predictor-corrector time-stepping is used.

In NB08, the 2D code was run for cases with different resistivities. It was found that if $\tau_c \ll \tau_R$, (τ_R is the characteristic resistive diffusion timescale), measured average rates of ohmic and viscous dissipation became insensitive to resistivity. A simple scaling analysis showed that this behavior could be derived beginning from general considerations if one includes the effects of the random walk nature of photospheric footpoint motions. However, because the simulations lacked instabilities or magnetic reconnection, the growth of magnetic energy was unbounded, with average transverse magnetic field \bar{B}_y scaling as $\eta^{-1/2}$. NB08 went on to demonstrate by further analytical argument that even if the growth of the magnetic field was thwarted, as would be the case in 3D simulations, dissipation would remain independent of resistivity, regardless of both the specific saturation level of B_\perp and of the mechanism causing the saturation. It is this conjecture we seek to examine.

The prescribed ordering $\tau_c \ll \tau_E$ (τ_E is the characteristic timescale over which energy is built up before being impulsively dissipated) is not met for the 3D simulations of Longcope & Sudan (1994), who found both dissipation and \bar{B}_y to scale as $\eta^{-1/3}$. For our numerical experiment, we extend the range they examined by an order of magnitude in either direction, establishing an adequate domain to assess the stated hypothesis. We have also adopted their footpoint braiding algorithm (as described in Longcope 1993), allowing a direct comparison of scaling results in the range they examined. Before proceeding with the details of our simulations, it is worth noting that NB08 demonstrated analytically as well as numerically that in the presence of steady footpoint motion, i.e., when $\phi(z = 0)$ and $\phi(z = L)$ are time-independent, the heating rate is inversely proportional to η , which is a strong and physically unrealistic dependence. For this reason, we do not pursue steady boundary flow, used in some other studies of coronal heating (e.g. Rappazzo et al. 2008).

3. NUMERICAL RESULTS: STATISTICAL STEADY STATE

We have performed a series of simulations using our 3D RMHD code described in Section 2 using a range of η spanning two orders of magnitude to study scaling laws. Extending the range in η by an order of magnitude beyond what was studied by Longcope & Sudan (1994) poses a significant challenge. As the dissipation coefficients (η and ν) get smaller, higher resolution has to be used to resolve smaller scales. To run the 3D code in high resolution, simulations are performed on parallel computers using MPI (Message Passing Interface). In order to run some cases for even longer time, we have also modified the code and run it on machines with GPUs (Graphics Processing Units) using Nvidia’s Compute Unified Device Architecture (CUDA).

The range of η has been extended to lower values (with $\tau_c = 10 \ll \tau_r$) for about an order of magnitude as compared with the study in Longcope & Sudan (1994) which stopped at $\eta \sim 10^{-3}$. This extension of course requires significant increase in resolution, with our highest resolution case at $512^2 \times 64$ so far (runs with even higher resolution, such as R0 in Table 1, have not been run for long enough time for good statistics), as compared with $48^2 \times 10$ in Longcope & Sudan (1994). The main diffi-

culty in performing these simulations is the requirement to run up to hundreds or even thousands of Alfvén times in order to obtain good statistics of the average quantities under the driving of random boundary flow. The basic parameters and results in this scaling analysis are summarized in Table 1.

It is crucial to the scaling study that we obtain good statistics averaging over time evolution in statistical steady state. As with previous long time integration studies of the Parker model, the runs are started with a uniform magnetic field along \hat{e}_z . After initial transients, the system will evolve to a statistical steady state. As mentioned above, thin current layers are formed and dissipated repeatedly during this statistical steady state. Figure 1 shows 3D iso-surfaces of J at a time taken from the R5 run, when there is a larger number of current sheets. This process is repeated indefinitely as the random boundary flows keep twisting the magnetic fields. Energy of the system is dissipated impulsively. As Poynting flux injection progressively braids the fields, energy is built up until an instability drives current sheet formation and reconnection, after which energy is released in a short time. This is a major characteristic of the statistical steady state. For the runs R5 (Blue) and R12 (Red), specified in Table 1, Figure 2 shows the intermittent nature of various quantities in time (in the unit of the Alfvén time τ_A , the time it takes for Alfvén waves to travel the distance of $L = 1$ between the two boundary plates along z).

Figure 2 (a) shows the total magnetic energy $E_M = \int \mathbf{B}_\perp^2 d^3x$, as well as total kinetic energy $E_K = \int \mathbf{v}_\perp^2 d^3x$, where the integration is over the 3D simulation box. Note that the magnetic energy does not include the contribution from the B_z component, which is constant in the RMHD model. Since the applied photospheric flow is chosen to be small (less than one tenth) compared with the Alfvén speed (with $\tau_c = 10\tau_A$), the magnetic field configuration maintains quasi-equilibrium for most of the time, except when strong current sheets form from time to time, thus inducing instabilities and strong dissipation. Therefore, E_M is usually much larger than E_K .

Figure 2 (b) shows the maximum current density J_{\max} over the whole 3D volume. J_{\max} increases over an order of magnitude on average in R5 compared with R12, and also fluctuates in time over a much larger amplitude. Observing Figures 2(a) and 2(b), note that the ratio of the increase in J_{\max} is much larger than the ratios of the increases of both E_M and E_K as η decreases.

Figure 2 (c) shows the ohmic dissipation $W_\eta = \eta \int J^2 d^3x$. Similarly, there is also energy dissipated by viscosity, at a rate given by $W_\nu = \nu \int \Omega^2 d^3x$ (not shown). Due to the same reason that E_K is much smaller than E_M , the viscous dissipation is much smaller than the ohmic dissipation, if we choose $\nu = \eta$ (Prandtl number equal to unity), which holds for most of our simulations. In this case, the total energy dissipation rate (heating rate) is dominated by ohmic dissipation. When we use values of ν greater than η , the viscous dissipation can become a more significant fraction of the ohmic dissipation. From the plot of W_η , we note that even though it shows large fluctuations in time, it fluctuates around a higher level for R5 than for R12 due to the smaller value of resistivity in the former.

To give a better measure of the level of energy dissipation, we can calculate the time averaged energy dissipation rates, e.g., $\bar{W}_\eta = [\int_0^t W_\eta dt']/t$, and similarly for \bar{W}_ν . The total energy dissipation rate is then $\bar{W} = \bar{W}_\eta + \bar{W}_\nu$, which is plotted in Figure 2(d). Our physical assumption here is that such averaged quantities will tend to saturated levels as t tends to infinity. In practice, since we can only simulate for finite time, such saturated levels are found at a time $t \gg \tau_c \gg \tau_A$ when these time-averaged values do not fluctuate too much. We do see from this plot that \bar{W} tends to saturate after a time much larger than τ_A .

Also plotted in Figure 2(d) is the time average Poynting flux \bar{I} , where $I = B_z \int \mathbf{v} \cdot \mathbf{B} d^2x$, integrated over the top and bottom boundary surfaces with $\mathbf{v} = \mathbf{u}_p$, the random photospheric flow. Note that I is not positive definite due to the fact that it involves the dot product between the velocity and magnetic field vectors and thus can be either positive or negative. However, the time averaged \bar{I} is almost always positive due to two factors. First, due to ohmic and viscous dissipation of energy into heat, if the total energy of the system is at a statistically steady level, there must be energy input from the boundary to provide this dissipation loss. Secondly, even when there is not much energy dissipation during a certain period, magnetic energy E_M generally increases, since the magnetic footpoints at the two boundaries connected to the same magnetic field line will move apart from each other in a random walk fashion due to random photospheric motion. Therefore, a typical field line will generally be stretched by the separation of the footpoints and the magnetic energy will increase. This increase in the magnetic energy must come from the Poynting flux. We see from Figure 2(d) that \bar{I} tends to saturate in the long-time limit at a level close to that of \bar{W} . In principle, these two rates should be the same, since the time averaged total energy also tends to a constant level. Numerically there is a slight difference between the two. Convergence studies show that this is mainly due to inaccuracy from finite grid size, and the difference decreases when higher resolution is used, especially in the parallel direction.

Another measure of the accuracy of our solutions is to test the energy balance equation,

$$\frac{d(E_M + E_K)}{dt} = I - W_\eta - W_\nu \quad (3)$$

Figure 2 (e) shows I as a function of time in pink for the run R5, $d(E_M + E_K)/dt$ (calculated by taking finite difference in time) in purple, $-W_\eta - W_\nu$ in blue, and the difference between the right and left hand sides of Equation (3) in green. We do see that the residual power due to numerical inaccuracy is generally small compared with other terms. While accuracy can be improved by running at higher resolutions, doing so would require much longer run times, as well as limit the highest Lundquist number that can be simulated. In the context of energy balance in our simulations, we remark that the energy dissipated due to ohmic or viscous terms is essentially converted into thermal energy. No energy term or transport equations are included. This is perhaps the primary weakness of this model, as it prevents us from predicting temperature and density profiles which can be directly compared with observations (see Dahlburg et al. 2009). However,

the heating rate required to maintain observed coronal temperatures can indeed be estimated as has been done in, e.g., Priest et al. (2002). NB08 followed this practice and found that the heating rate determined from 2D simulations is consistent with such estimation, if the energy dissipation does turn into heat as assumed. Readers should compare similarities and differences between this treatment with those used in other studies (Longcope 1993; Longcope & Sudan 1994; Rappazzo et al. 2008; Hendrix & van Hoven 1996; Hendrix et al. 1996; Galsgaard & Nordlund 1996; Rappazzo et al. 2010).

Figure 2 (f) shows \bar{B}_\perp as a function of time. Here \bar{B}_\perp is defined as a root-mean-square value of the magnetic field strength, and so is effectively the square root of E_M per unit volume. Similar to other time-averaged quantities, \bar{B}_\perp also tends to saturate at long time, at values that are much more physically reasonable than those in the 2D runs. We remark that these saturated levels in the 3D runs are already much more reasonable than those in the 2D runs that were found to have a scaling of $\bar{B}_\perp \propto \eta^{-1/2}$, which can be much larger than unity (the value of the constant B_z used in the simulations). Thus, inclusion of 3D effects is seen to reduce the magnitude of \bar{B}_\perp to values that are smaller than the magnitude of B_z .

These effects include the formation of thin current layers, onset of instabilities, and subsequent reconnection and enhanced energy dissipation. All these effects are more prominent when B_\perp is larger, effectively limiting the growth of B_\perp . Thus, these 3D effects can self-regulate the level of B_\perp that can be built up when subjected to the driving of the random footpoint motion.

Due to the fact that we are injecting energy into the system through random photospheric footpoint motion, a natural question to ask is whether this would induce other random processes, such as a turbulent cascade of energy that contributes to the heating of the corona. Indeed, turbulence has been studied in various coronal loop heating models beginning with the early work of van Ballegooyen (1986) and more recently by others (Hendrix et al. 1996; Dmitruk et al. 1998; Rappazzo et al. 2008). However, as mentioned in the above discussion, we are driving with slow boundary flows (less than 1/10 of the Alfvén speed) with $\tau_c \gg \tau_A$, and thus the magnetic field configuration maintains quasi-equilibrium most of the time. Moreover, we apply random boundary flows, instead of constant motion as in, e.g., Rappazzo et al. (2008), so that energy injection is much slower due to the fact that magnetic field lines are stretched in a random walk fashion rather than at a constant rate. As a result, we have $E_K \ll E_M$, which is not consistent with equipartition of energy in Alfvén wave turbulence. Similar to Hendrix et al. (1996), energy spectra in our simulations are largely exponential (not shown here) during relatively quiescent periods, with little or no impulsive energy release, but become progressively shallow power laws during particularly intense current sheet disruption events, with possible excitation of more Alfvén waves for a short duration. As with their study however, computation grid resolutions enable us to resolve less than a decade of the inertial range of the energy cascade.

While it seems turbulence plays just a minor role in our present analysis, whether it plays a crucial role in determining the speed of magnetic reconnection has at-

tracted a number of recent investigations (e.g. Lazarian & Vishniac 1999; Loureiro et al. 2007; Bhattacharjee et al. 2009; Loureiro et al. 2009; Kowal et al. 2009). It is evident there is a surge of interest in numerical experiments concerning turbulent reconnection and that much has yet to be settled. It would be interesting to see if any insights can be gleaned from our own data. As mentioned above, the presence of turbulence seems to be intermittent in our simulations, mainly during intense impulsive current sheet disruption events. Of crucial importance here is how well resolved we can be, and therefore how well developed an inertial range we can identify. This will depend on how low the value of η (and thus how high the Lundquist number S) we can simulate in 3D, as well as how important physical properties scale with η or S , which we turn our attention to now.

Figure 3 shows some of the scaling results we have obtained so far. In Figure 3 (a), the time-averaged ohmic dissipation rate \bar{W}_η (at the saturated level) for different η for the runs listed in Table 1 is plotted in triangles, while the viscous dissipation rate \bar{W}_ν are plotted in squares. As pointed out above, $\bar{W}_\nu \ll \bar{W}_\eta$ in general, and thus the total dissipation rate (heating rate) $\bar{W} = \bar{W}_\eta + \bar{W}_\nu$ (plotted in asterisks) is very close to \bar{W}_η , except in the large resistivity limit. The time-averaged Poynting flux \bar{I} is also plotted in the same graph in circles. It should be the same value as \bar{W} theoretically, and we do see that the differences between these two quantities are generally small in our numerical results, indicating acceptable accuracy.

From this plot, we see that \bar{W} actually only changes within an order of magnitude, and levels off at both the large and small η limit. This has important implications for the coronal heating problem, since the Lundquist number (on the order of the inverse of the normalized η in our simulations) can be as high as 10^{14} in the solar corona. Therefore, the leveling off of \bar{W} at the small η limit is especially important, and is in fact predicted by NB08 based on 2D simulations and theoretical arguments. As mentioned above, this level of \bar{W} was shown in NB08 to be independent of dissipation mechanism provided that the correlation time τ_c is small compared with the time to build up magnetic energy. It was also estimated that this level of heating rate can give the same order of magnitude required for realistic coronal heating, following similar considerations as in Priest et al. (2002). However, the amount of magnetic energy built up in this process does depend on dissipation mechanism, and becomes unphysically large in 2D simulations in the small η limit (with \bar{B}_\perp scaling as $\eta^{-1/2}$). We will now show that this scaling becomes much weaker in 3D.

Figure 3 (b) shows the time-averaged \bar{B}_\perp (at the saturated level) for different η . This is a measure of the magnetic field (or magnetic energy) production in the statistical steady state due to the applied random photospheric motion. Unlike \bar{W} , \bar{B}_\perp production changes over an order of magnitude from large to small η . This is because in the highly resistive limit, magnetic field produced is quickly dissipated and can only reach a low magnitude, while the dissipation rate does not decrease that much. In the small resistivity limit, the increase of \bar{B}_\perp slows down significantly.

Due to the fact that we are doing 3D simulations, and

that we need to simulate for a long time to obtain good statistics, so far we have only been able to extend the value of η to about an order of magnitude lower, as compared with similar studies in (Longcope & Sudan 1994). Nevertheless, we can see already that below $\eta \sim 10^{-3}$, there is a significant deviation from the scalings obtained in Longcope & Sudan (1994), who showed by numerical computation and scaling analysis that both \bar{W} and \bar{B}_\perp should scale with $\eta^{-1/3}$ in the small η limit. We have added dotted lines in Figure 3 (a) and (b) showing the $\eta^{-1/3}$ scaling. We see that the portion of the data in a range close to $\eta \sim 10^{-3}$ is indeed consistent with an $\eta^{-1/3}$ scaling. However, as described above, both \bar{W} and \bar{B}_\perp increase much slower with decreasing η for even smaller η . This result has important implications on the solar coronal heating problem, since the Lundquist number in the solar corona is very high and hence we most likely need to have a mechanism to provide coronal heating that is independent of the Lundquist number in order to obtain a physically reasonable heating rate. At the same time, the magnetic field energy production should not increase to an unreasonable level compared with observations. In addition to this numerical evidence, we will provide our own scaling analysis to make sense of these results, as well as compare with results in Longcope & Sudan (1994).

4. SCALING ANALYSIS

We have shown an initial confirmation of the hypothesis of NB08 but as an additional goal we would like to understand the exact mechanism giving rise to saturation. Their conjecture made clear that the insensitivity to η holds true no matter what the saturation mechanism is. In order to provide a more complete numerical confirmation of their conjecture, it becomes necessary to identify the possible physical mechanisms behind saturation.

A natural place to begin would be to examine the results of Longcope (1993) and Longcope & Sudan (1994) who derived scaling laws based on Sweet–Parker reconnection theory and analyzed a range in η which we have covered in our own study. By looking at where their scaling behavior or where their assumptions might be failing in our own numerical results, we might gain some insight into the physics occurring at even lower η . The reader is referred to these papers for a detailed review of their scaling arguments. Here we will only discuss their assumptions and results briefly.

They assumed Sweet–Parker theory is valid in the sense that when looking at only the current sheet region forming between two coalescing islands (flux tubes), the reconnection can be treated as a steady process in resistive MHD which results in the classic Sweet–Parker scaling relating the width δ and length Δ of a reconnecting current sheet:

$$\delta/\Delta \sim S_\perp^{-1/2} \quad (4)$$

where $S_\perp \equiv \bar{B}_\perp w/\eta$ is the perpendicular Lundquist number, with w being the perpendicular length scale of the reconnecting islands and so $w \sim v_p \tau_c$ with v_p being the root-mean-square value of the random photospheric flow velocity. They also observed that both the number of current sheets N in the simulation box and the length of

the current sheets Δ are relatively insensitive to resistivity. We follow these assumptions as a starting point for our discussion, although we recognize that some of them need to be re-examined more carefully in future studies.

In particular, the Sweet–Parker reconnection theory should apply only to higher Lundquist number (smaller η) cases, in which the energy dissipation is dominated by the reconnection process. Therefore, the scaling analysis presented here should not work for larger η (i.e. $\eta > 0.01$ here), which is actually not within the focus of our studies here. When the energy dissipation is mainly from the Sweet–Parker current sheets, the dissipation rate can be estimated by

$$\bar{W} \sim \eta N \Delta L \frac{\bar{B}_\perp^2}{\delta} \sim \frac{\bar{B}_\perp^2 L L_\perp^2}{\tau_E} \quad (5)$$

where we have used the estimation that the current density of the current sheet is given by $J \sim \bar{B}_\perp/\delta$ and that the volume of the simulation box is $L L_\perp^2$. The energy dissipation timescale τ_E in Equation (5) can then be solved as

$$\tau_E \sim L_\perp^2 / N(\eta w \bar{B}_\perp)^{1/2} \quad (6)$$

where we have used the Sweet–Parker scaling in Equation (4). In a statistical steady state, the energy dissipation by Equation (5) has to be replenished by the production of magnetic field energy due to the footpoint motion within the same amount of time τ_E .

In the studies of Longcope (1993) and Longcope & Sudan (1994), although random photospheric motion was used in the simulations, the effects due to such random flows were not taken into account in their scaling analysis. This can be justified if τ_c is much larger than the energy dissipation time τ_E . In this case, the magnetic field strength production is given by

$$\bar{B}_\perp \sim B_z \frac{v_p \tau_E}{L} \sim \left[\left(\frac{B_z v_p}{L N} \right)^2 \frac{L_\perp^4}{w \eta} \right]^{1/3} \quad (7)$$

where we have used Equation (6) and solved for \bar{B}_\perp . Putting back Equation (7) into Equation (6) results in

$$\tau_E \sim \left(\frac{L_\perp^4 L}{N^2 w B_z v_p \eta} \right)^{1/3} \quad (8)$$

and so the energy dissipation rate becomes

$$\bar{W} \sim \left(\frac{L_\perp^{10} B_z^5 v_p^5}{L^2 N^2 w \eta} \right)^{1/3} \quad (9)$$

after putting Eqs. (7) and (8) into Equation (5). Note that all three of these quantities, \bar{B}_\perp , τ_E , and \bar{W} scale with $\eta^{-1/3}$, and thus we have recovered scaling laws derived in Longcope (1993) and Longcope & Sudan (1994), although we are using a slightly different approach.

We may now put reasonable numbers into Eqs. (7) to (9) and compare with our simulation results. Our simulations are set up to use $L = L_\perp = B_z = 1$. The root-mean-square photospheric flow velocity is measured numerically to be $v_p \sim 0.075$, and thus $w \sim v_p \tau_c = 0.75$. The average number of current sheets N is more difficult to determine and is subject to some uncertainties. However, we have done some analysis (not shown here) of our

simulations for different η and found that $N \sim 7$ numerically in the small η limit. This seems to be somewhat higher than expected from the number of reconnecting islands (flux tubes). However, it is actually quite common to see multiple current sheets in a simulation output, as shown in Figure 1.

Based on these values, we have $\tau_E \sim 0.71/\eta^{1/3}$, and so $\tau_E \sim 7.1$ for $\eta = 10^{-3}$. At the same time we get $\bar{B}_\perp \sim 0.53$ from Equation (7), and $\bar{W} \sim 0.04$ from Equation (9) at the same η . Both of these are close enough to the values found in Figure 3 (a) and (b), and so it is an indication that our parameters used in these estimations are consistent with simulations. Compared with the value of $\tau_c = 10$, we see that although τ_E is still smaller than τ_c , it is about the same order of magnitude and thus Equation (7) is only marginally justified. For larger η , τ_E is smaller, e.g., $\tau_E \sim 3.3$ for $\eta = 0.01$ and thus is much smaller than τ_c so that the random effect is not as important. This qualitatively explains why we see from Figure 3 (a) and (b) that there is a range roughly around $\eta \sim 0.01$ to 0.001 where both \bar{W} and \bar{B}_\perp scale approximately as $\eta^{-1/3}$, as indicated by the two dotted lines in the two plots. However, for smaller η , τ_E becomes larger, e.g., $\tau_E \sim 15$ for $\eta = 10^{-4}$ (if we continue to use the approximation, which may not be strictly valid), and thus larger than τ_c which makes the effect of randomness important. This explains the deviation from the $\eta^{-1/3}$ scaling for both \bar{W} and \bar{B}_\perp for η smaller than around 10^{-3} .

Now, taking into account the effect of random boundary flow, which makes the footpoints move in a random walk fashion as argued in NB08, the estimate for magnetic field production must be changed from Equation (7) to

$$\bar{B}_\perp \sim B_z \frac{v_p(\tau_c \tau_E)^{1/2}}{L} \sim \left[\left(\frac{B_z v_p L_\perp}{L} \right)^4 \frac{\tau_c^2}{N^2 w \eta} \right]^{1/5} \quad (10)$$

where we have again used Equation (6) and solved for \bar{B}_\perp . Substituting Equation (10) back into Equation (6) results in

$$\tau_E \sim \left[\frac{L_\perp^8}{N^4 \tau_c} \left(\frac{L}{w B_z v_p \eta} \right)^2 \right]^{1/5} \quad (11)$$

and so the energy dissipation rate becomes

$$\bar{W} \sim \frac{L_\perp^2}{L} B_z^2 v_p^2 \tau_c \quad (12)$$

after putting Eqs. (10) and (11) into Equation (5), and thus it is independent of η . Note that Equation (12) is exactly the same as found in NB08 for systems regardless of dissipation mechanism, and is estimated to give the same order of heating consistent with observations.

Using the same values of L , L_\perp , B_z , τ_c , v_p , w , and N , Equation (11) becomes $\tau_E \sim 0.42/\eta^{2/5}$, and thus $\tau_E \sim 6.7$ for $\eta = 10^{-3}$, if we could apply this equation. This turns out to be very close to $\tau_E \sim 7.1$ estimated above using Equation (8), indicating that the transition point between these two regimes of scalings is around $\eta = 10^{-3}$ in our simulations. For $\eta = 10^{-4}$, Equation (11) gives $\tau_E \sim 17$, which is significantly larger than τ_c , and so

these scalings based on random walk of footpoints are justified.

Based on this set of parameters, Equation (12) predicts $\bar{W} \sim 0.056$ (independent of η), which is close to the asymptotic values found in Figure 3 (a) in the small η limit. We do see from this plot that \bar{W} indeed does not increase as fast when η is below 10^{-3} , and is consistent with a trend to a constant level in small η , although we still only have a limited range of η that we can simulate. At the same time, Equation (10) gives a value of $\bar{B}_\perp \sim 0.97$, which is somewhat larger than expected from Figure 3 (b), although we do need to recognize that there are uncertainties in these scaling estimates.

A better test of Equation (10) would be the scaling with η in the small η limit. In Figure 3 (b), we have also plotted a dashed line indicating the scaling of $\eta^{-1/5}$. We do see that this seems to be consistent with a portion of the data of \bar{B}_\perp below $\eta \sim 10^{-3}$. However, we cannot rule out the possibility that \bar{B}_\perp is actually increasing slower than $\eta^{-1/5}$, possibly due to a modification of the Sweet–Parker reconnection scalings, e.g., Equation (4). We will further discuss this possibility in the next section.

5. DISCUSSION AND CONCLUSION

In this paper, we have presented our latest results based on numerical simulations of a 3D RMHD solar corona heating model for a range of η (and thus Lundquist number) with random photospheric motion. These simulations were performed over a period of more than two years and numerical results have been verified carefully to eliminate possible errors. So far, we have been able to simulate cases with η about an order of magnitude smaller than those presented in similar studies in (Longcope 1993) and (Longcope & Sudan 1994). While this extension seems modest, it actually requires much more computational effort due to the increase in resolution and running time required, as well as the decrease of time-step for numerical stability. To be able to achieve that, we have been running our simulations in parallel computers, as well as using GPUs.

Moreover, we have shown that the extension of this scaling study towards smaller η turns out to have very important physical consequences. Numerically, we have shown that the scaling laws (with \bar{W} and \bar{B}_\perp scale with $\eta^{-1/3}$) found in Longcope (1993) and Longcope & Sudan (1994) become invalid for η smaller than what was used in their studies (around $\eta \sim 10^{-3}$). Both \bar{W} and \bar{B}_\perp are now found to increase much more slowly for smaller η , with \bar{W} possibly leveling off to an asymptotic value. We have presented our own scaling analysis to justify our numerical results. By following similar assumptions as in Longcope (1993) and Longcope & Sudan (1994), e.g., using Sweet–Parker scalings, we have been able to recover their $\eta^{-1/3}$ scaling laws for a range of η larger than 10^{-3} . We have demonstrated that the transition between scaling behaviors derives from the fact that the effects of random photospheric motion are not important in the larger η range where the energy dissipation time τ_E is smaller than the correlation time τ_c of the random flow. For η smaller than around 10^{-3} , τ_E becomes comparable or even larger than τ_c . In this range, an analysis based on the random walk of photospheric footpoints motion will predict the insensitivity to η we observe, further substan-

tiating the results found in NB08 which were based on 2D simulations and more general theoretical considerations. This is important to the problem of coronal heating since this heating rate has been shown to be consistent with the requirements for coronal heating.

We have also shown that now \bar{B}_\perp has a much weaker scaling with η , i.e., $\eta^{-1/5}$ instead. This is much better than the $\eta^{-1/2}$ scaling in 2D simulations, as well as weaker than the $\eta^{-1/3}$ scaling found in Longcope (1993) and Longcope & Sudan (1994). This means that this scaling will predict a more physically realistic level of magnetic field as compared with observations. However, due to the fact that the Lundquist number of (\sim inverse of η) the solar corona can be very high (up to $10^{12} - 10^{14}$), even a $\eta^{-1/5}$ scaling would result in an unrealistically large magnetic field, despite a much weaker dependence. The reason behind this is the fact that the Sweet–Parker reconnection rate, which scales with $\eta^{1/2}$ is too slow for high Lundquist numbers.

One solution for this problem is the possibility of a higher rate of magnetic reconnection even under resistive MHD. This possibility has attracted a number of recent investigations (e.g., Lazarian & Vishniac 1999; Loureiro et al. 2007; Bhattacharjee et al. 2009; Loureiro et al. 2009; Kowal et al. 2009). Many of these studies fall within the scope of turbulent reconnection. While there are some indications that \bar{B}_\perp found in our simulations might actu-

ally scale weaker than even $\eta^{-1/5}$, we still have not been able to simulate even smaller η to confirm this definitively. Moreover, the effects due to turbulence are still too difficult to study using our current level of resolution. However, this question is important enough that we are trying different ways to extend our range of η to even smaller values to study these effects.

In summary, by simulating with η about an order of magnitude smaller than in previous studies, we have been able to find new physical effects due to random photospheric flows and thus new scalings with Lundquist number. In future work, with further improvements in our computational approach, we hope to report results with even smaller values of η , and investigate the possibilities of another asymptotic range involving secondary instabilities and turbulent processes.

The authors thank Matt Gilson for his contribution in programming a part of the code as a summer student project. Computer time was provided by UNH (using the Zaphod Beowulf cluster at the Institute for the Study of Earth, Oceans and Space), as well as grants of HPC resources from the Arctic Region Supercomputing Center, the DoD High Performance Computing Modernization Program, and NSF TeraGrid resources provided by NCSA. This research is supported in part by grants from NSF (AGS-0962477 and AGS-0962698), NASA (NNX08BA71G, NNX09AJ86G, and NNX10AC04G) and DOE (DE-FG0207ER46372).

REFERENCES

- Aschwanden, M. J. 2004, *Physics of the Solar Corona. An Introduction*, ed. Aschwanden, M. J. (Praxis Publishing Ltd)
- Bhattacharjee, A., Huang, Y., Yang, H., & Rogers, B. 2009, *Phys. Plasmas*, 16, 112102
- Dahlburg, R. B., Rappazzo, A. F., & Velli, M. 2010, *AIP Conf. Proc.*, 1216, Twelfth International Solar Wind Conference, ed. M. Maksimovic et al. (Melville, NY: AIP), 40
- Dmitruk, P., Gómez, D. O., & Deluca, E. E. 1998, *ApJ*, 505, 974
- Einaudi, G., Velli, M., Politano, H., & Pouquet, A. 1996, *ApJ*, 457, L113
- Galsgaard, K., & Nordlund, Å. 1996, *J. Geophys. Res.*, 101, 13445
- Gomez, D. O., Dmitruk, P. A., & Milano, L. J. 2000, *Sol. Phys.*, 195, 299
- Gudiksen, B. V., & Nordlund, Å. 2005, *ApJ*, 618, 1020
- Hendrix, D. L., & van Hoven, G. 1996, *ApJ*, 467, 887
- Hendrix, D. L., van Hoven, G., Mikic, Z., & Schnack, D. D. 1996, *ApJ*, 470, 1192
- Huang, Y.-M., Bhattacharjee, A., & Zweibel, E. G. 2010, *Phys. Plasmas*, 17, 055707
- Janse, Å. M., Low, B. C., & Parker, E. N. 2010, *Phys. Plasmas*, 17, 092901
- Kadomtsev, B. B., & Pogutse, O. P. 1974, *Sov. J. Exp. and Theor. Phys.*, 38, 283
- Klimchuk, J. A. 2006, *Sol. Phys.*, 234, 41
- Kowal, G., Lazarian, A., Vishniac, E. T., & Otmianowska-Mazur, K. 2009, *ApJ*, 700, 63
- Lazarian, A., & Vishniac, E. T. 1999, *ApJ*, 517, 700
- Lee, J.-Y., Barnes, G., Leka, K. D., Reeves, K. K., Korreck, K. E., Golub, L., & DeLuca, E. E. 2010, *ApJ*, 723, 1493
- Longcope, D. W. 1993, Ph.D. thesis, Cornell Univ.
- Longcope, D. W., & Sudan, R. N. 1994, *ApJ*, 437, 491
- Loureiro, N. F., Schekochihin, A. A., & Cowley, S. C. 2007, *Phys. Plasmas*, 14, 100703
- Loureiro, N. F., Uzdensky, D. A., Schekochihin, A. A., Cowley, S. C., & Yousef, T. A. 2009, *MNRAS*, 399, L146
- Low, B. C. 2010, *ApJ*, 718, 717
- Mikic, Z., Schnack, D. D., & van Hoven, G. 1989, *ApJ*, 338, 1148
- Ng, C. S., & Bhattacharjee, A. 1998, *Phys. Plasmas*, 5, 4028
- Ng, C. S., & Bhattacharjee, 2008, *ApJ*, 675, 899
- Ng, C. S., Rosenberg, D., Pouquet, A., Germaschewski, K., & Bhattacharjee, A. 2008, *ApJS*, 177, 613
- Parker, E. N. 1972, *ApJ*, 174, 499
- Parker, E. N. 1979, *Cosmical Magnetic Fields: Their Origin and Their Activity* (New York: Oxford University Press)
- Parker, E. N. 1983, *ApJ*, 264, 635
- Parker, E. N. 1983, *ApJ*, 264, 642
- Parker, E. N. 1988, *ApJ*, 330, 474
- Parker, E. N. 1994, *Spontaneous current sheets in magnetic fields : with applications to stellar x-rays.* (International Series in Astronomy and Astrophysics, Vol. 1. New York: Oxford University Press)
- Peter, H., Gudiksen, B. V., & Nordlund, Å. 2006, *ApJ*, 638, 1086
- Priest, E. R., Heyvaerts, J. F., & Title, A. M. 2002, *ApJ*, 576, 533
- Priest, E. R., Longcope, D. W., & Heyvaerts, J. 2005, *ApJ*, 624, 1057
- Rappazzo, A. F., Velli, M., & Einaudi, G. 2010, *ApJ*, 722, 65
- Rappazzo, A. F., Velli, M., Einaudi, G., & Dahlburg, R. B. 2008, *ApJ*, 677, 1348
- Reale, F. 2010, *Living Rev. Sol. Phys.*, 7, 5
- Strauss, H. R. 1976, *Phys. Fluids*, 19, 134
- van Ballegooijen, A. A. 1986, *ApJ*, 311, 1001

TABLE 1
SUMMARY OF NUMERICAL RUNS

Run	η	ν	B_{\perp}	S_{\perp}	W_{η}	W_{ν}	Poynting	T/τ_A	Resolution
R0	0.00015625	0.00015625	0.542	3470	0.0446	0.0103	0.0587	305.545	$1024^2 \times 128$
R1	0.00015625	0.00015625	0.537	3440	0.0468	0.0127	0.0546	487.252	$512^2 \times 64$
R2	0.00015625	0.00062500	0.610	3900	0.0513	0.0283	0.0519	245.546	$512^2 \times 32$
R3	0.00015625	0.00062500	0.614	3930	0.0498	0.0275	0.0458	77.0269	$512^2 \times 32$
R4	0.00031250	0.00031250	0.492	1570	0.0433	0.00792	0.0491	857.407	$512^2 \times 64$
R5	0.00031250	0.00031250	0.503	1610	0.0452	0.00941	0.0478	9321.75	$256^2 \times 32$
R6	0.00031250	0.00062500	0.502	1610	0.0431	0.0111	0.0467	2032.02	$256^2 \times 32$
R7	0.00062500	0.00062500	0.449	718	0.0416	0.00540	0.0427	19342.8	$128^2 \times 32$
R8	0.00062500	0.00062500	0.448	717	0.0399	0.00502	0.0401	820.339	$128^2 \times 32$
R9	0.0012500	0.0012500	0.372	298	0.0370	0.00332	0.0385	11668.2	$128^2 \times 32$
R10	0.0012500	0.0012500	0.371	297	0.0373	0.00336	0.0411	706.141	$64^2 \times 16$
R11	0.0025000	0.0025000	0.279	112	0.0299	0.00272	0.0311	1317.70	$64^2 \times 16$
R12	0.0050000	0.0050000	0.183	36.7	0.0215	0.00317	0.0252	2566.96	$64^2 \times 16$
R13	0.0100000	0.0100000	0.103	10.3	0.0132	0.00394	0.0168	5209.60	$64^2 \times 16$
R14	0.020000	0.020000	0.0547	2.73	0.00822	0.00511	0.0123	10245.4	$64^2 \times 16$
R15	0.040000	0.040000	0.0307	0.767	0.00623	0.00544	0.0113	10240.3	$32^2 \times 64$
R16	0.080000	0.080000	0.0197	0.246	0.00550	0.00612	0.0105	10240.5	$32^2 \times 64$

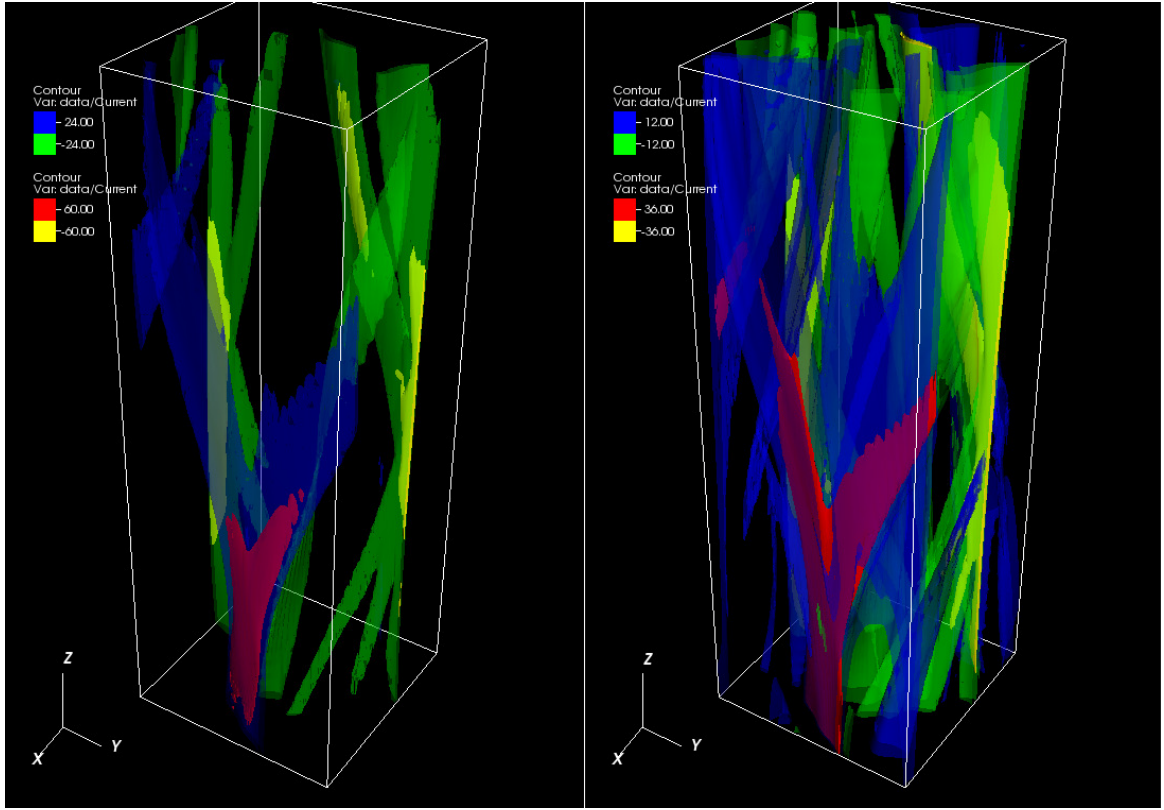


FIG. 1.— 3D iso-surfaces of J at a time taken from the R7 run. Both figures are from the same time sample for the R7 run. The left panel shows iso-surfaces at $J = -60, -24, 24, 60$ while the right panel shows iso-surfaces at $J = -36, -12, 12, 36$. Blue and green iso-surfaces are made semi-transparent for greater visibility.

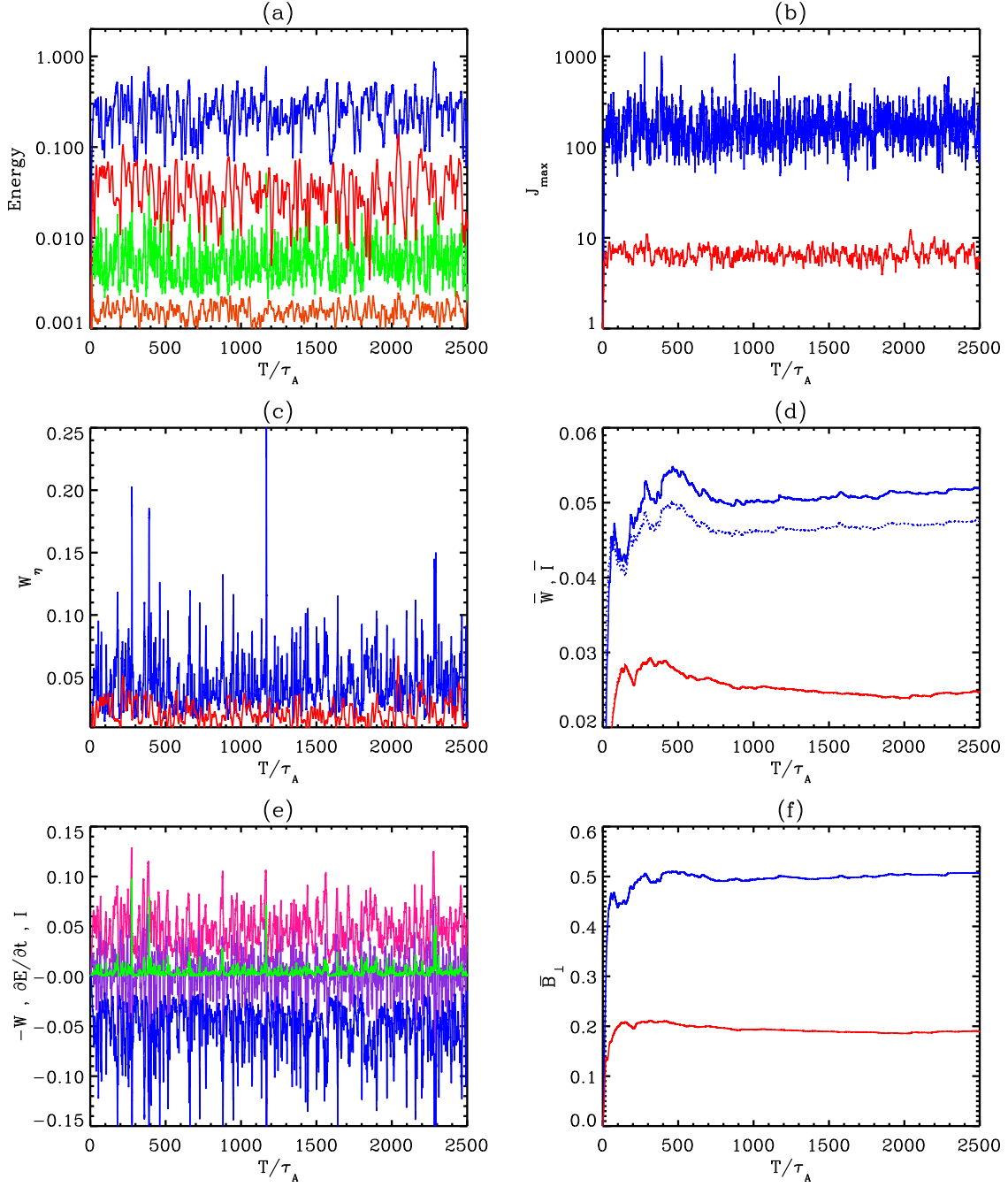


FIG. 2.— Plots (a), (b), (c), (d), and (f) show time series of various quantities for runs R5 (Blue) and R12 (Red). In (a), green and orange correspond to E_K for R5 and R12 respectively while blue and red show E_M . For plot (d), solid lines show \bar{W} and dotted lines show \bar{I} . For run R5 plot (e) shows $-W = -(W_\eta + W_\nu)$ (Blue), I (Pink), $d(E_M + E_K)/dt$ (Purple), and the difference between the right and left hand sides of Equation 3 (Green). Parameters used for these runs can be found in Table 1.

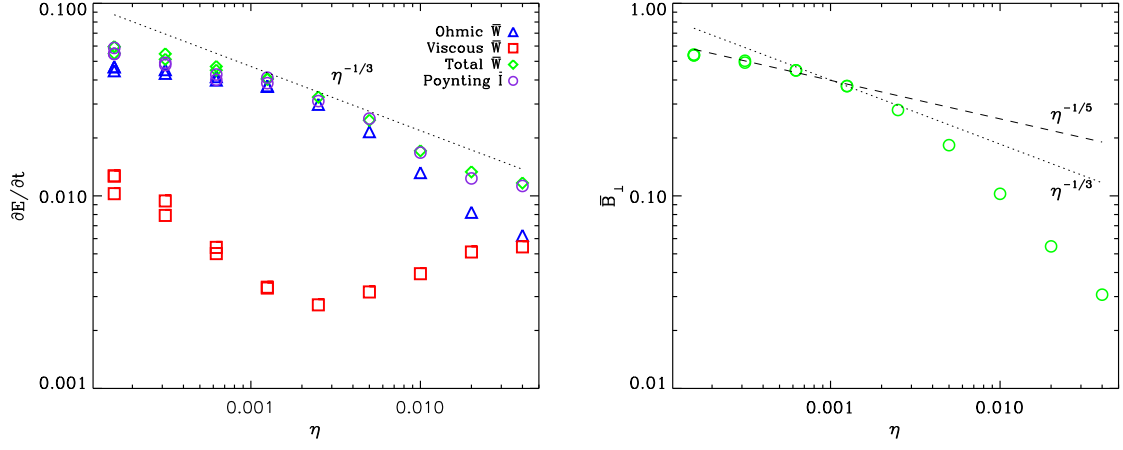


FIG. 3.— (a) Average energy dissipation rate for different values of η . \triangle is ohmic dissipation, \square is viscous dissipation, \diamond is the total of the two, and \circ is the footpoint Poynting flux. (b) Average perpendicular magnetic field strength for different values of η .